AGU PUBLICATIONS

Geophysical Research Letters

RESEARCH LETTER
10.1002/2015GL065465

Special Section:
First Results from the MAVEN Mission to Mars

Water and water ions in the Martian thermosphere/ionosphere

Jane L. Fox[1], M. Benna[2,3], P. R. Mahaffy[3], and B. M. Jakosky[4]

[1]Department of Physics, Wright State University, Dayton, Ohio, USA, [2]CRESST, University of Maryland, Baltimore County, Catonsville, Maryland, USA, [3]NASA Goddard Space Flight Center, Greenbelt, Maryland, USA, [4]Laboratory for Atmospheric and Space Physics, University of Colorado Boulder, Boulder, Colorado, USA

Key Points:
- We preset the first model of water in the Martian thermosphere
- The predicted density profiles of H_2O, H_2O^+, and H_3O^+ are presented
- We predict that H_2^+ is the mass-2 ion rather than D^+

Correspondence to:
J. L. Fox,
jane.fox@wright.edu

Citation:
Fox, J. L., M. Benna, P. R. Mahaffy, and B. M. Jakosky (2015), Water and water ions in the Martian thermosphere/ionosphere, *Geophys. Res. Lett.*, *42*, doi:10.1002/2015GL065465.

Received 22 JUL 2015
Accepted 17 SEP 2015

Abstract First results from the Neutral Gas and Ion Mass Spectrometer instrument on the Mars Atmosphere and Volatile EvolutioN (MAVEN) spacecraft reveal density profiles of protonated species that are mostly in good qualitative agreement with recent models of the Martian thermosphere/ionosphere. We present here the first photochemical model in which the density profiles of water and water ions in the ionosphere/thermosphere are predicted. We find that the computed peak densities of OH^+, H_2O^+, and H_3O^+ are in fairly good agreement with the measured values. The computed column density of water is predicted to be about 10^{10} cm^{-2}, and the mixing ratio at 80 km is 0.4 ppb. The actual water densities must be small enough so that HCO^+ is not destroyed by proton transfer to water during the daytime and large enough so that H_3O^+ dominates the ionosphere at low altitudes just beyond the terminator. The calculations also show that the mass-2 ion is almost certainly H_2^+.

1. Introduction

Most of water in the Martian atmosphere is confined to the region below the condensation level, which usually is found between the surface and 40 km, although it may be higher during global dust storms [e.g., *Jakosky*, 1985]. Water is assumed to be well mixed in this region. In models of the middle atmosphere, water is assumed to be present at the saturation vapor pressure from the condensation level up to fairly high altitudes, usually in the 60 to 100 km range [e.g., *Anbar et al.*, 1993; *Nair et al.*, 1994; *Krasnopolsky*, 1993, 2006, 2011; *Zhu and Yee*, 2007; *Rodrigo et al.*, 1990]. We note here that the minimum temperature in our model is ~140 K from 80 to 100 km. The saturation vapor pressure of water at this temperature is equivalent to a rather large number density of about 10^8 cm^{-3}, which corresponds to a mixing ratio of ~ 3 ppm at 80 km, the lower boundary of our model.

In the middle atmosphere of Mars water is photolyzed by solar FUV photons longward of about 1500 Å:

$$H_2O + h\nu \rightarrow OH + H. \quad (1)$$

This process initiates the production of odd-hydrogen species (HO_x) in the middle atmosphere. Odd-hydrogen radicals catalyze the recombination of CO and O, which are produced by photolysis of CO_2.

Water is assumed not to be present in most of the existing thermospheric models. H_2 is predicted to be the most abundant hydrogen species in the middle and upper atmosphere. It is produced from reactions of odd-hydrogen species derived from water. H_2 is assumed to be transported upward to the thermosphere, where it is photodissociated and participates in ion-molecule reactions in which atomic H is formed.

Rodrigo et al. [1990] constructed a model of the Martian atmosphere in which they investigated the chemistry of odd-hydrogen and odd-oxygen radicals and their long-lived tracers. They predicted density profiles of H_2, H_2O, and H from 30 km to 200 km. By assuming that its thermospheric profile is determined only by eddy and molecular diffusion, they predicted an H_2O number density at 80 km of about 1×10^5 cm^{-3} or a mixing ratio of about 3 ppb.

In the present study, we construct the first model of the density profiles of water vapor, H_2O, and the water ions, H_2O^+ and H_3O^+, in the Martian thermosphere/ionosphere in which the production and loss of these species by photochemistry is included. For the ions, we also include ambipolar diffusion, and for minor

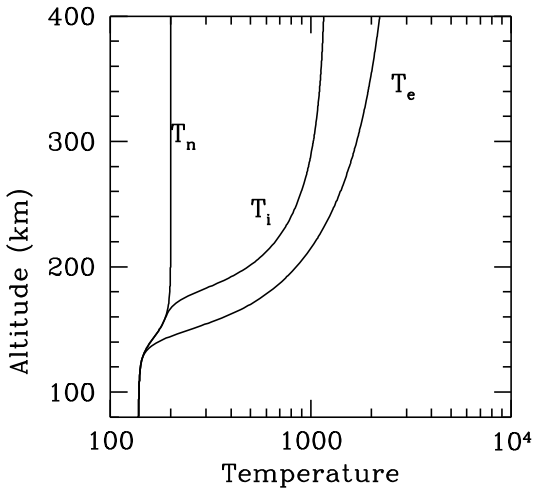

Figure 1. Neutral, ion, and electron temperature profiles adopted in this model. The values for T_i and T_e were smoothed from those previously used in our models but were not taken from actual data.

neutrals, we include eddy diffusion and molecular diffusion. By imposing a zero velocity upper boundary condition on H_2O and a zero flux lower boundary condition, we determine the density profile of neutral water that is produced by ion-molecule reactions alone.

For this first report, we have adopted the pre-MAVEN low solar activity 60° SZA neutral model of *Fox* [2009, 2015], and therefore, our results should be considered to be illustrative only. In the future, we will construct a more realistic model, in which we will adopt neutral densities as measured by the Neutral Gas Ion Mass Spectrometer (NGIMS) [e.g., *Mahaffy et al.*, 2015], solar fluxes derived from the measurements of the EUV monitor on the Langmuir Probe and Waves (LPW) instrument [e.g., *Eparvier et al.*, 2015], ion temperatures (T_i) from the Suprathermal and Thermal Ion Composition (STATIC) instrument [*McFadden et al.*, 2015], and electron temperatures (T_e) from the LPW instrument [e.g., *Ergun et al.*, 2015]. Previously, we computed the density profiles of 10 protonated species, including HCO^+, $OCOH^+$, OH^+, N_2H^+, H_3^+, HO_2^+, HNO^+, ArH^+, CH^+, and H_2^+. The chemical reactions and the rate coefficients involving these species are enumerated by *Fox* [2015].

In addition to H_2O^+ and H_3O^+, we have recently added to the model NH^+ and HOC^+, with reaction rate coefficients taken from the University of Manchester Institute of Science and Technology database [*McElroy et al.*, 2013] and the compilation of ion-molecule reactions of *Anicich* [2003]. For the new dissociative recombination reactions, we adopt rate coefficients from the review of *Florescu-Mitchell and Mitchell* [2006].

The shapes of the ion density profiles at high altitudes are determined by multiple factors, including the shapes of the T_i and T_e profiles. We have here smoothed the plasma temperature profiles so that they do not exhibit the slope discontinuities of the Viking profiles. Our adopted temperature profiles are shown in Figure 1.

2. Chemistry of Water and Water Ions

In the cold dense clouds of the interstellar medium (ISM) water is produced mainly via ion-molecule reactions. Water ions have been predicted to play an important role in determining the chemical distribution of oxygen-containing species in the ISM and other astrophysical environments [e.g., *van Dishoeck and Black*, 1986; *Dalgarno and Fox*, 1994]. Very recently, these predictions have been confirmed by direct observation of OH^+, H_2O^+, and H_3O^+ [e.g., *Indriolo et al.*, 2015, and references therein]. We adopt here the reactions that are important in the ISM, and we add several more that are specific to the Martian ionosphere.

The basic principles of chemistry of ions on Mars have been described in general terms by *Fox* [2015]. For atmospheres that contain even a small amount of hydrogen, including Mars, many ions are protonated species that are produced and destroyed by proton transfer and other reactions. For these species, ionization flows from ions whose parent neutrals have smaller proton affinities (PAs) to those whose parent neutrals have larger PAs. The proton affinities are given in the critical compilation of *Hunter and Lias* [1998]. H_2O has the largest PA, 7.24 eV, of the important species of the Martian thermosphere. In the absence of water, and where there are sufficient collisions, HCO^+ is the terminal ion. We define terminal ions as those that are destroyed mainly via dissociative recombination (DR) reactions, which result in production of neutrals. Because these ions have few loss processes, they also tend to have longer chemical lifetimes than other ions. The PA of CO, for H^+ attached to the C atom, is 6.16 eV. C has a larger proton affinity than CO, about 6.46 eV, but there is little C in the Martian thermospheric model, and therefore, CH^+ is predicted to be a minor ion. The densities of $OCOH^+$ are also predicted to be relatively large at low altitudes, due mostly to production by reaction of CO_2^+ with H_2. The proton affinity of CO_2 is relatively large, about 5.67 eV.

Photochemical production of H_2O^+ and H_3O^+ ions may begin with formation of O^+ by a number of mechanisms, including photoionization or electron-impact ionization of O or via charge transfer reactions. Once formed, O^+ initiates a series of abstraction reactions that form the intermediates OH^+ and H_2O^+ and that terminate in H_3O^+:

$$O^+ + H_2 \rightarrow OH^+ + H, \quad (2)$$

$$OH^+ + H_2 \rightarrow H_2O^+ + H, \quad (3)$$

and

$$H_2O^+ + H_2 \rightarrow H_3O^+ + H. \quad (4)$$

As the terminal ion, H_3O^+ in the Martian ionosphere is destroyed only by DR:

$$H_3O^+ + e \rightarrow H + H_2O, \quad (5a)$$

$$H_3O^+ + e \rightarrow OH + H_2, \quad (5b)$$

$$H_3O^+ + e \rightarrow OH + H + H. \quad (5c)$$

$$H_3O^+ + e \rightarrow H_2 + O + H. \quad (5d)$$

Channel (5a) produces H_2O, but the branching ratio for that channel is small, of the order of 0.2–0.3.

Other paths to H_2O^+ include

$$H_3^+ + O \rightarrow H_2O^+ + H, \quad (6)$$

which competes with

$$H_3^+ + O \rightarrow OH^+ + H_2. \quad (7)$$

Proton transfer to OH is a possible source of H_2O^+, but we do not yet include OH in our thermospheric model.

In the Martian ionosphere H_2O^+ may be destroyed by DR or by proton transfer to any species that has a larger proton affinity than that of OH (6.14 eV), such as C, CO, or H_2O:

$$H_2O^+ + C \rightarrow CH^+ + OH, \quad (8)$$

$$H_2O^+ + CO \rightarrow HCO^+ + OH, \quad (9)$$

and

$$H_2O^+ + H_2O \rightarrow H_3O^+ + OH, \quad (10)$$

respectively. H_2O^+ also may be destroyed by charge transfer to any species that has a smaller ionization potential (IP) than that of H_2O (12.61 eV), forming neutral H_2O in the process. In the Martian ionosphere, only the minor species O_2 and NO have smaller IPs than H_2O.

If neutral water vapor is present in sufficient quantities, H_2O^+ may be formed in charge transfer to H_2O by ions X^+, whose parent neutrals have larger IPs than that of H_2O. These reactions can be represented as

$$X^+ + H_2O \rightarrow X + H_2O^+, \quad (11)$$

where X^+ may be He^+, Ar^+, N_2^+, H_2^+, N^+, CO^+, CO_2^+, O^+, H^+, or OH^+.

In the Martian thermosphere, water vapor is subject to direct ionization, dissociative ionization, or dissociation by solar photons or photoelectrons. In these interactions, a variety of fragments, such as H, O, and OH, and fragment ions, such as H^+, OH^+, and O^+, are produced. We have included in our model photoionization, photodissociative ionization, and photodissociation of H_2O with cross sections from *Verner et al.* [1996], *Chan et al.* [1993], *Yoshino et al.* [1996, 1997], and *Parkinson and Yoshino* [2003]. For electron-impact processes, we have adopted the cross sections from *Harb et al.* [2001], *Kedzierski et al.* [1998], *Hwang et al.* [1996] and the compilation of *Itikawa and Mason* [2005].

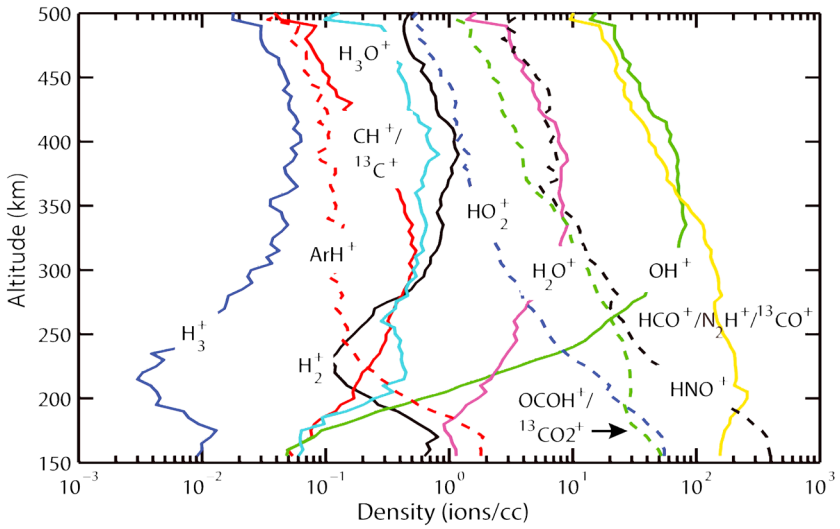

Figure 2. Altitude profiles of the measured densities of protonated species from the NGIMS instrument on MAVEN. These densities are averaged values in 5 km bins for the 60–65° solar zenith angle (SZA) range.

3. Results

In Figure 2 we present altitude profiles of the averaged density measurements of protonated species measured by the NGIMS instrument on MAVEN in the 60°–65° solar zenith angle (SZA) range [*Benna et al.*, 2015]. These densities are averages of all the measurements in 5 km bins. Most of the profiles of water ions, H_2O^+, H_3O^+, the intermediate OH^+, and CH^+, exhibit a peak between 300 and 400 km. Those of other protonated species decrease monotonically with increasing altitude, such as HO_2^+, HNO^+, and ArH^+. The density profile of the mass-29 ion represents the sum of HCO^+, N_2H^+, HOC^+, and $^{13}CO^+$, and its structure is difficult to characterize.

Since we have not yet adopted the neutral densities from the NGIMS measurements, our computed profiles should be taken as semiquantitative only. In previous models, we have imposed an upward velocity boundary condition on the ions in order to fit the Viking 1 density profiles of O_2^+, O^+, and CO_2^+ for the low solar activity model [*Hanson et al.*, 1977]. Such a boundary condition does not, however, reproduce the O_2^+ profiles measured by the NGIMS instrument. Therefore, we here impose a zero upward velocity boundary condition on all the ions. This assumption produces an upper limit to the ion densities at high altitudes. If we impose even a small upward velocity on the ions at the top of the model at 400 km, the high-altitude ion peaks decrease slightly in both altitude and density, and the production rate of H_2O decreases. Obviously, we need to raise the top altitude of our model to about 500 km in order to characterize the high altitude behavior of the ion density profiles.

The present model includes 28 ions, 14 of which are protonated species, including H_2O^+ and H_3O^+. We have also computed the densities of 10 minor neutral species, 9 of which we have included in previous models; here we have added water vapor [e.g., *Fox*, 2015, and references therein]. The upper boundary condition on the neutrals is zero velocity, except for H and H_2, for which Jeans velocities of 216 and 0.613 cm s^{-1}, respectively, are imposed at 400 km.

Our model results are shown in Figures 3a–3d. Figure 3a shows the density profiles for 12 of the 14 ions that have been previously modeled from 80 to 400 km [e.g., *Fox*, 2009]. The O^+ profile shown is the sum of $O^+(^4S)$, $O^+(^2D)$, and $O^+(^2P)$, which we compute separately. A comparison of the O_2^+ and O^+ profiles with those from the NGIMS as presented by *Benna et al.* [2015] shows that the model O_2^+ and O^+ densities diverge seriously from the measured values. The measurements show that the densities of O_2^+ fall off rather steeply above 150 km, and the O^+ densities peak at about 1000 cm^{-3} in the 250–350 km range; they appear to merge with the O_2^+ densities near 300 km. Our computed O^+ density is about 540 cm^{-3} near 300 km, where the O_2^+ density is, however, ~2900 cm^{-3}.

The computed total ion density peak is apparently too high and too large in our model. Multiple factors determine the altitude and magnitude of the O_2^+ peak, including the neutral density profiles, the neutral and plasma

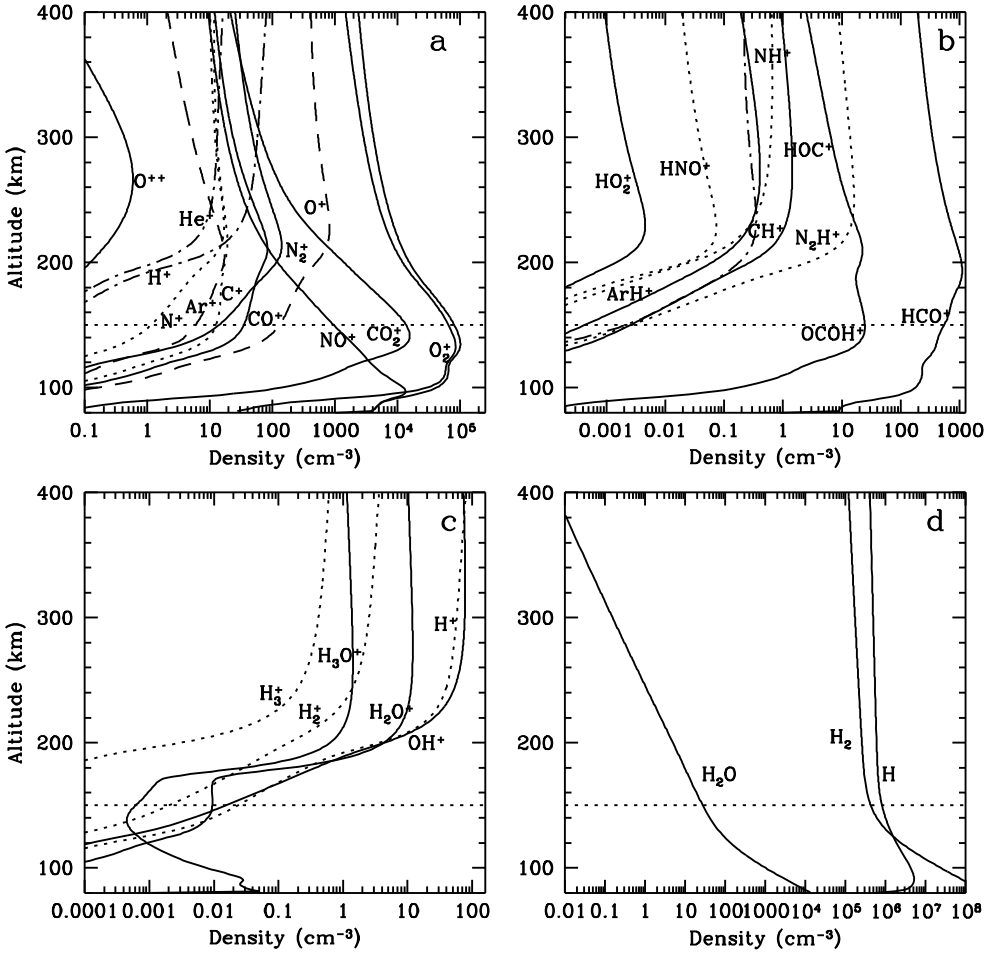

Figure 3. Predicted ion density profiles for our model thermosphere/ionosphere. The horizontal dotted line in each panel shows the nominal periapsis of the MAVEN spacecraft at 150 km. (a) Twelve ions that were previously in our model. (b) Nine protonated species. The N-bearing ions are shown by dotted curves, and CH^+ is shown with a dash-dotted curve for clarity. (c) Density profiles of hydrogen ions and the analogous water ions. The solid curves represent the H- and O-containing ions, and the dashed curves represent ions that contain only H atoms. (d) Computed density profiles for H, H_2, and H_2O.

temperatures, and the solar fluxes. We have adopted the Solar2000 (S2K) v1.24 model for day 200 of 1976 [e.g., *Tobiska*, 2004]. This particular model exhibits fluxes in the short wavelength regions that are elevated compared to those of other low solar activity models, such as the S2K v2.22 fluxes used by *Fox* [2009].

The difference between the measured and model electron densities at 150 km is large. The NGIMS total ion densities at that altitude are of the order of 2×10^4 cm^{-3}, whereas our model values are about 8×10^4 cm^{-3}. With revised solar fluxes and neutral densities taken from MAVEN data, our O_2^+ density profiles should be in better agreement with the data. Since DR is the main loss mechanism for O_2^+ and DR coefficients have negative temperature dependencies, smaller values for T_e would also reduce the O_2^+ peak density. We note here, however, that the normalization of the NGIMS ion densities to the LPW electron densities has not yet been finalized.

The predicted density profiles of nine protonated species are shown in Figure 3b, and those of hydrogen and water ions are shown in Figure 3c. The model predicts that the major mass-29 ion is HCO^+. The computed high-altitude values of most of the ions are in qualitative agreement with the measured values, but at low altitudes, they diverge. Several differences between the measured and model density profiles of the protonated species are evident. We focus here on the water ions and hydrogen ions, and we will defer discussion of the other protonated species to a later investigation.

Predicted density profiles of the hydrogen ions, H_n^+, and water ions, H_nO^+, where $n = 1-3$, are presented in Figure 3c. The computed density profile of OH^+ ions exhibits a peak near 325 km of about 78 cm^{-3}, in acceptable agreement with that from the NGIMS data, for which the peak density is about 80 cm^{-3} near 350 km. The computed density profile of H_2O^+ exhibits a peak near 280 of about 12 cm^{-3}, whereas the measured value shown in Figure 2 is about 10 cm^{-3} near 350 km. The predicted H_3O^+ density peak is about 1.4 cm^{-3}, whereas the measured values peak at about 1 cm^{-3} near 400 km, in satisfactory agreement. If water is formed only by ion chemistry, then H_2O^+ and H_3O^+ will be found mostly at high altitudes and in small quantities.

The computed H_2^+ density profile attains a value of about 3.6 cm^{-3} at 400 km, whereas the measured mass-2 ion density peaks at a value that is slightly larger than 1 cm^{-3} near 400 km. The predicted density profile of H^+ peaks near 400 km with a density of about 80 cm^{-3}. NGIMS cannot measure the mass-1 ion densities. The D/H ratio in water vapor was measured by the Sample Analysis at Mars instrument on the rover Curiosity and was found to be about 6 times the value in Standard Mean Ocean Water or about $\sim 9.3 \times 10^{-4}$ [e.g, *Webster et al.*, 2013]. The atmospheric D/H ratio is determined by several processes, some of which increase the fraction of D in the atmosphere, such as escape to space, and some of which favor H, such as photolysis of HDO/H_2O and HD/H_2. The chemistries of H^+ and D^+ should be similar. If we consider the measured D/H ratio near the surface as an upper limit for D^+/H^+ in the ionosphere, then the model D^+ peak density would be less than ~ 0.1 cm^{-3}. This shows convincingly that the mass-2 ion is H_2^+ rather than D^+.

In Figure 3d, we show our computed densities for neutral H, H_2, and H_2O. The computed H_2O profile shows the amount of water that can be produced through ion chemistry, without transport from below. The water vapor density at 80 km is about 1.4×10^4 cm^{-3}, which represents a mixing ratio of about 0.4 ppb. The computed total column density of water above 80 km is about 1×10^{10} cm^{-2}. The low-altitude secondary peak of H_3O^+ in the model reflects its production from proton transfer to ambient water.

Maltagliati et al. [2013] reported retrievals of the water vapor distributions in the atmosphere of Mars below 50–100 km, using the infrared solar occultation technique with the Spectroscopie pour l'Investigation des Charactéristiques Atmosphériques de Mars instrument on the Mars Express Spacecraft, with a sensitivity of the order of 1 ppm. They showed that there are strong variations in the water vapor distribution at different seasons and latitudes. The mixing ratios were found to fall off sharply on the topsides, but some of the retrievals showed mixing ratios of a few parts per million near 80 km with very large error bars. Apparently, the water abundances at altitudes above 50 km were difficult to measure. A mixing ratio of 1 ppm at 80 km corresponds to a very large number density of water, more than $\sim 3 \times 10^7$ cm^{-3}. This is more than 3 orders of magnitude larger than our predictions of the water abundance at 80 km. Even a mixing ratio of $\sim$ 3 ppb, as suggested by the model of *Rodrigo et al.* [1990] would alter the photochemistry of protonated species, especially that of water ions. We would expect the terminal ion, H_3O^+, to become more important in the lower ionosphere, especially as the solar zenith angle increases near and just beyond the terminator.

In Figure 4, we show two-dimensional plots of O^+, OH^+, H_2O^+, $OCOH^+$, H_3O^+, and HCO^+ as a function of altitude from 130 or 150 km to 500 km in 5 km bins. The SZAs range from 0° to ~125° in 5° bins. H_3O^+ and HCO^+ are produced from species that have the highest proton affinities of all the neutrals in the Martian thermosphere, and therefore, they have the longest lifetimes. Since H_3O^+ is destroyed only by DR in the Martian ionosphere, its specific loss rate is given by $\mathcal{L} = \alpha n_e$, where α is the DR coefficient and n_e is the electron density. The chemical lifetime of a species is $\tau_c = 1/\mathcal{L}$. On the dayside, the value of $\mathcal{L}$ for H_3O^+ is largest in the region of the electron density peak. Thus, reduced values for τ_c explain the smaller densities of H_3O^+ on the dayside.

This effect can be seen in Figure 4 (bottom row), which indicate that the largest densities of HCO^+ and H_3O^+ can be found at lower altitudes at larger SZAs. The diminished solar flux in this region leads to a reduction in the ambient electron densities. This reduces the specific loss rates of the terminal ions HCO^+ and H_3O^+ and increases their photochemical lifetimes; thus, their densities also increase. For H_3O^+, this effect is dependent on the existence of a sufficient supply of water vapor at lower altitudes. It appears that the amount of water that can be produced photochemically above 80 km may be insufficient to explain the low-altitude densities beyond the terminator. On the other hand, the densities of water must be small enough so that HCO^+ is not destroyed completely. The actual abundance of water vapor in the thermosphere is bracketed by these two requirements. Further modeling will elucidate these effects.

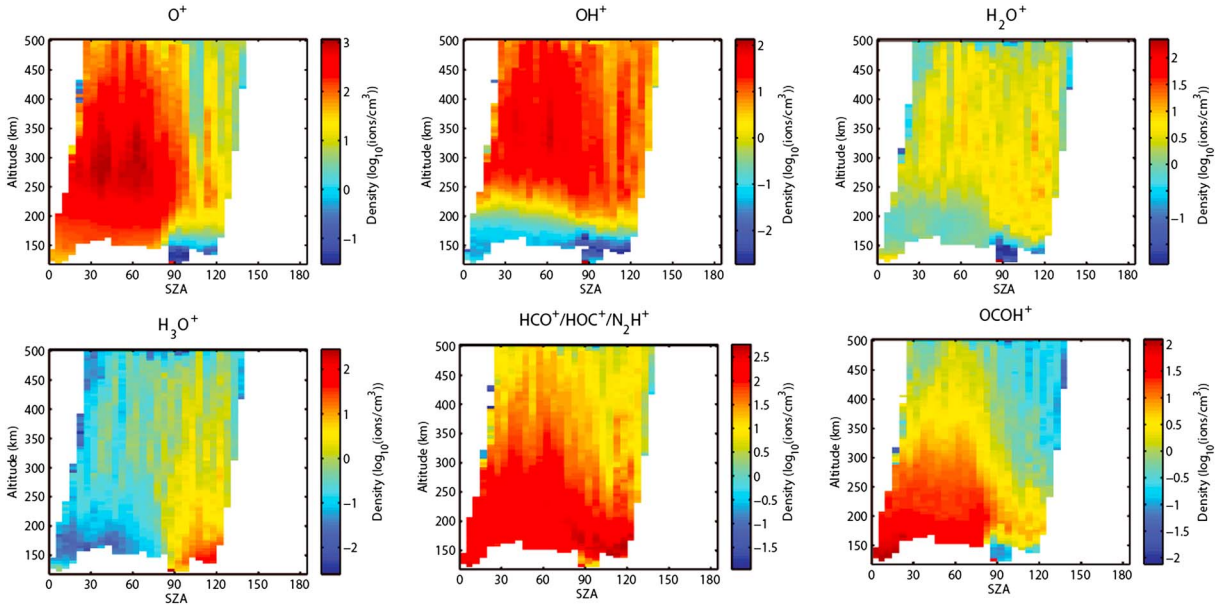

Figure 4. Spatial distribution of O^+, OH^+, H_2O^+, H_3O^+, HCO^+, and $OCOH^+$ as a function of altitude and solar zenith angle as measured by NGIMS. Each plot represents the full data set acquired from 18 October 2014 to 18 May 2015. The observations were binned as a function of altitude in 5 km intervals and in 5° SZA intervals.

On the nightside, the ionosphere may be maintained up to ~125° SZA by day-to-night transport of O^+ and O_2^+ [e.g., *Duru et al.*, 2011; *Cui et al.*, 2015]. O_2^+ is not involved in this chemistry to a great extent; its major loss processes at low altitudes are charge transfer to NO, reaction with N and DR [e.g., *Fox and Sung*, 2001]. O^+, however, initiates the production of water ions via the reaction sequence (2) to (4). Protonated species that are not terminal ions are characterized by smaller lifetimes and will transfer their protons to CO or H_2O, or undergo other reactions that ultimately produce HCO^+ or H_3O^+. Eventually these ions, if not replenished on the nightside by ion transport or energetic electron precipitation, will undergo DR and disappear.

In our model, the densities of HCO^+ at 150 km are larger than those measured by factors of about 3. If there were more water in the thermosphere than in our model, HCO^+ ions would be destroyed in proton transfer reactions to H_2O, forming H_3O^+. In Figure 2, the measured H_2O^+ densities can be seen to decrease with increasing altitude for about 30 km above 150 km. It is not, however, clear whether this feature is the beginning of a peak or is noise in the data. If the former, then this H_2O^+ could be a result of direct ionization of water.

4. Summary and Conclusions

We have modeled the thermosphere/ionosphere of Mars from 80 to 400 km for 60° SZA. Our model contains 13 background species, and we compute the density profiles of 28 ions, including 14 protonated species. Previously, we have computed the density profiles of 10 protonated species [*Fox*, 2015]. To the nine minor neutrals, whose densities we have predicted in previous models, we add here neutral water vapor. By imposing a zero flux boundary condition on the water at 80 km, and zero velocity at 400 km, we calculate the H_2O densities that can be produced photochemically, rather than those in which the source of water is assumed to be transportation from below. This investigation represents the first photochemical model calculation of water vapor in the thermosphere and of ionized water, H_2O^+, and protonated water, H_3O^+, in the ionosphere. Calculations of the density profiles of H-containing ions, H_n^+ where $n = (1-3)$, show convincingly that the measured mass-2 ion is H_2^+, rather than D^+.

We predict an H_2O density at 80 km of 1.4×10^4 cm^{-3} and a column density of about 10^{10} cm^{-2}. The predicted mixing ratio at 80 km is ~0.4 ppb, which is small compared to those assumed at the upper boundaries of models of the middle atmosphere. The large H_3O^+ densities measured by NGIMS at low altitudes beyond the terminator suggest that the computed water abundance may be insufficient. The other protonated species would be expected to transfer a proton to H_2O. The presence of HCO^+ in the same region shows, however,

that there is not a very large amount of water present in the thermosphere, which would destroy this ion by proton transfer reactions. These two requirements bracket the thermospheric abundance of H_2O.

For the protonated species other than the terminal ions, the most important loss mechanisms are ion-molecule reactions, rather than DR. These species have shorter chemical lifetimes than do the terminal ions. As the solar flux decreases and the thermosphere goes into shadow these species may not be replenished by photochemistry, although the nightside ionosphere may be maintained by ion transport to ~125° SZA. Our calculations predict that the most important protonated species on the dayside at low altitudes is HCO^+.

This first model is based, however, upon neutral density profiles from Viking 1 and on fairly arbitrary smoothed and revised ion and electron temperatures. The boundary conditions at the top of the model for all the ions and most of the neutrals are zero velocities, and thus, the predicted ion and water densities at high altitudes are upper limits. A more realistic model calculation is in progress in which we adopt MAVEN in situ data, and we extend the top of the model to 500 km.

Acknowledgments
We thank the reviewers for their careful reading of the manuscript. The MAVEN mission has been funded by NASA through the Mars Exploration Program.

The Editor thanks John Black and Matthew Fillingim for their assistance in evaluating this paper.

References

Anbar, A. D., M. Allen, and H. Nair (1993), Photodissociation in the atmosphere of Mars: Impact of high resolution, temperature-dependent CO_2 cross sections, *J. Geophys. Res.*, *98*, 10,925–10,931.

Anicich, V. G. (2003), *An Index of the Literature for Bimolecular Gas Phase Cation-Molecule Reaction Kinetics*, JPL Publ., 03-19, Pasadena, Calif.

Benna, M., P. R. Mahaffy, J. M. Grebowsky, J. L. Fox, R. V. Yelle, and B. M. Jakosky (2015), First measurements of composition and dynamics of the Martian ionosphere by MAVEN's Neutral Gas and Ion Mass Spectrometer, *Geophys. Res. Lett.*, *42*, doi:10.1002/2015GL066146.

Chan, W. F., G. Cooper, and C. E. Brion (1993), The electronic spectrum of water in the discrete and continuum region: Absolute optical oscillator strengths for photoabsorption (6–200 eV), *Chem. Phys.*, *178*, 387–400.

Cui, J., M. Galand, R. V. Yelle, Y. Wei, and S.-J. Zhang (2015), Day-to-night transport in the Martian ionosphere: Implications from total electron content measurements, *J. Geophys. Res. Space Physics*, *120*, 2333–2346, doi:10.1002/2014JA020788.

Dalgarno, A., and J. L. Fox (1994), Ion chemistry in atmospheric and astrophysical plasmas, in *Unimolecular and Bimolecular Ion-Molecule Reaction Dynamics*, edited by C.-Y. Ng, T. Baer, and I. Powis, pp. 1–85, Wiley, Chichester, U. K.

Duru, F., D. A. Gurnett, D. D. Morgan, J. D. Winningham, R. A. Frahm, and A. F. Nagy (2011), Nightside ionosphere of Mars studied with local electron densities: A general overview and electron density depressions, *J. Geophys. Res.*, *116*, A10316, doi:10.1029/2011JA016835.

Florescu-Mitchell, A. I., and J. B. A. Mitchell (2006), Dissociative recombination, *Phys. Rep.*, *430*, 277–374.

Eparvier, F. G., P. C. Chamberlin, T. N. Woods, and E. M. B. Thiemann (2015), The solar extreme ultraviolet monitor for MAVEN, *Space. Sci. Rev.*, doi:10.1007/s11214-015-0195-2.

Ergun, R. E., et al. (2015), Dayside electron temperature and density profiles at Mars: First results from the MAVEN LPW instrument, *Geophys. Res. Lett.*, *42*, doi:10.1002/2015GL065280.

Fox, J. L. (2009), Morphology of the dayside ionosphere of Mars: Implication for ion outflows, *J. Geophys. Res.*, *114*, E12005, doi:10.1029/2009JE003432.

Fox, J. L. (2015), Chemistry of protonated species in the Martian ionosphere, *Icarus*, *252*, 366–392, doi:10.1016/j.icarus.2015.01.010.

Fox, J. L., and K. Y. Sung (2001), Solar activity variations in the Venus ionosphere/thermosphere, *J. Geophys. Res.*, *106*, 21,305–21,335.

Hanson, W. B., S. Sanatani, and D. R. Zuccaro (1977), The Martian ionosphere as observed by the Viking retarding potential analyzers, *J. Geophys. Res.*, *82*, 4351–4367.

Harb, T., W. Kedzierski, and J. M. McConkey (2001), Production of ground state OH following electron impact on H_2O, *J. Chem. Phys.*, *115*, 5507–5512.

Hunter, E. P. L., and S. G. Lias (1998), Evaluated gas phase basicities and proton affinities of molecules: An update, *J. Phys. Chem. Ref. Data*, *27*, 413–656.

Hwang, W., Y.-K. Kim, and M. E. Rudd (1996), New model for electron-impact ionization cross sections of molecules, *J. Chem. Phys.*, *104*, 2956–2966.

Indriolo, N., et al. (2015), HERSCHEL Survey of galactic OH^+, H_2O^+, and H_3O^+: Probing the molecular hydrogen fractions and cosmic-ray ionization rate, *Astrophys. J.*, *800*, 40, doi:10.1088/0004-637X/800/1/40.

Itikawa, Y., and N. Mason (2005), Cross sections for electron collisions with water molecules, *J. Phys. Chem. Ref. Data*, *34*, 1–22.

Jakosky, B. M. (1985), The seasonal cycle of water on Mars, *Space Sci. Rev.*, *41*, 131–200.

Kedzierski, W., J. Derbyshire, C. Malone, and J. W. McConkey (1998), Isotope effects in the electron-impact break up of water, *J. Phys. B.*, *31*, 5361–5368.

Krasnopolsky, V. A. (1993), Photochemistry of the Martian atmosphere (mean conditions), *Icarus*, *101*, 313–332.

Krasnopolsky, V. A. (2006), Photochemistry of the Martian atmosphere: Seasonal, latitudinal, and diurnal variations, *Icarus*, *185*, 153–170.

Krasnopolsky, V. A. (2011), Atmospheric chemistry on Venus, Earth, and Mars, *Icarus*, *59*, 952–964.

Mahaffy, P. R., et al. (2015), Structure and composition of the neutral upper atmosphere of Mars from MAVEN NGIMS investigation, *Geophys. Res. Lett.*, *42*, doi:10.1002/2015GL065329.

Maltagliati, L., et al. (2013), Annual survey of water vapor vertical distribution and water–aerosol coupling in the martian atmosphere observed by SPICAM/MEx solar occultations, *Icarus*, *223*, 942–962.

McElroy, D., C. Walsh, A. J. Markwick, M. A. Cordiner, K. Smith, and T. J. Millar (2013), The UMIST database for astrochemistry 2012, *Astron. Astrophys.*, *550*(A36), 1–13, doi:10.1051/0004-6361/201220465.

McFadden, J., et al. (2015), Structure and composition of the Martian ionosphere and atmospheric loss: MAVEN STATIC first results, *Abstract 2899*, Lunar Planet. Sci. Conf., The Woodlands, Tex.

Nair, H., M. Allen, A. D. Anbar, and Y. L. Yung (1994), A photochemical model of the Martian atmosphere, *Icarus*, *111*, 124–150.

Parkinson, W. H., and K. Yoshino (2003), Absorption cross-section measurements of water vapor in the wavelength range 181–199 nm, *Chem. Phys.*, *294*, 31–35.

Rodrigo, R., E. García-Álvarez, M. J. Lopez-Gonzalez, and J. J. López-Moreno (1990), A non-steady one-dimensional theoretical model of Mars' neutral atmospheric composition between 30 and 200 km, *J. Geophys. Res.*, *95*, 14,795–14,810.

Tobiska, W. K. (2004), SOLAR2000 irradiances for climate change, aeronomy and space system engineering, *Adv. Space. Res.*, *34*(8), 1736–1746.

van Dishoeck, E. F., and J. H. Black (1986), Comprehensive models of diffuse interstellar clouds: Physical conditions and molecular abundances, *Astrophys. J. Suppl. Ser.*, *62*, 109–145.

Verner, D. A., G. J. Ferland, K. T. Korista, and D. G. Yakovlev (1996), Atomic data for astrophysics. II. New analytic fits for photoionization cross sections of atoms and ions, *Astrophys. J.*, *465*, 487–498.

Webster, C. R., et al. (2013), Isotope ratios of H, C, and O in CO_2 and H_2O of the Martian atmosphere, *Science*, *341*, 260–263.

Yoshino, K., J. R. Esmond, W. H. Parkinson, K. Ito, and T. Matsui (1996), Absorption cross section measurements of water vapor in the wavelength region 120 to 188 nm, *Chem. Phys.*, *211*, 387–391, doi:10.1016/0301-0104(96)00210-8.

Yoshino, K., J. R. Esmond, W. H. Parkinson, K. Ito, and T. Matsui (1997), Erratum: Absorption cross section measurements of water vapor in the wavelength region 120 to 188 nm, *Chem. Phys.*, *215*, 429–430, doi:10.1016/S0301-0104(96)00381-3.

Zhu, X., and J.-H. Yee (2007), Wave-photochemistry coupling and its effect on water vapor, ozone and airglow variations in the atmosphere of Mars, *Icarus*, *189*, 136–150.